Kerbala Journal of Pharmaceutical Sciences

ISSN: 2221-7207(Print) / **ISSN**: 3006-7189 (Online)

Mechanisms of Drug Resistance in Leishmania Parasites: From Transporter Genes to Host Cell Reprogramming

Israa Mohammad Abd AL-Khaliq[1]*& Mai Khalil Ismail[2]

[1] HLA Typing Unit, Al-Kindy College of Medicine, Baghdad University, Baghdad, Iraq.

[2]Clinical Immunology, College of Science, University of Baghdad

[*]**Corresponding author**

Israa Mohammad Abd AL-Khaliq: israamohammad@kmc.eubaghdad.edu.iq.

Received: 28/03/2026
Accepted: 25/05/2026
Published: 30/06/2026

Keywords: *Leishmania Donovani*, Antimonial resistance, Aquaglyceroporin AQP1, Translational reprogramming, Macrophage polarization.

DOI:10.62472/kjps.v17.i28.171-186

Abstract

The resistances to drugs that occur through changes in the Leishmania parasites are making global health increasingly precarious, and limiting the ability to manage clinically visceral leishmaniasis and cutaneous leishmaniasis. The work detailed in this study combines molecular and cellular investigations of several layers of drug resistance via antimony (Sb) in *Leishmania donovani* by considering components involved in this resistance – from membrane-bound transporters to changes in translation of proteins to metabolic manipulation of host macrophages. Using lines of sensitive (S-strain) and resistant (R-strain) *L. donovani* that were derived from clinical isolates or developed in the laboratory, we examined drug accumulation over time, the expression of specific genes, the translational activity of these genes and the polarization of the macrophage's immune system. Our results were quantified by inductively coupled plasma mass spectrometry (ICP-MS) and showed that R-strains accumulate 74.1% less intracellular tri-valent antimony at physiological temperatures; this was due to the down-regulation of the aquaglyceroporin 1 (AQP1) gene transcript between 65-78%. In addition, the MRP (multidrug resistance protein (ABCB5)) ABC-transporter was up-regulated 5.12 times allowing the sequestration of metal-thiol conjugates in the intracellular environment. Overall polysome profiling and quantitative proteomic analysis of translation initiation factors indicated that S-strains translate proteins during oxidative stress and R-strains, during oxidative stress, undergo translational reprogramming and maintain the translation of survival proteins by going around the phosphorylation of eIF2-alpha. At the host-parasite interface, using R-strain infected macrophages showed an anti-inflammatory M2-type polarization, with decreases in TNF-alpha of 55% and increases in IL-10 of 2.4 times. Collectively, these results demonstrate that drug resistance to antimony is more than just a transport barrier – it is a coordinated systemic response at several levels that completely alters both the proteome of the parasite and the immunological landscape of the host.

آليات مقاومة الأدوية في طفيليات الليشمانيا: من جينات الناقلات إلى إعادة برمجة الخلايا المضيفة"

اسراء محمد عبد الخالق، مي خليل اسماعيل

المستخلص

إن مقاومة الأدوية التي تحدث نتيجة التغيرات في طفيليات الليشمانيا تجعل الصحة العالمية في وضع حرج بشكل متزايد، وتحد من القدرة على الإدارة السريرية لمرض الليشمانيا الحشوية والليشمانيا الجلدية. يجمع العمل المفصل في هذه الدراسة بين الاستقصاءات الجزيئية والخلوية لعدة مستويات من مقاومة الأدوية عبر مركب الأنتيمون (Sb) في طفيلية *الليشمانيا الدونوفانية* (*Leishmania donovani*)، وذلك من خلال النظر في المكونات المشاركة في هذه المقاومة – بدءًا من الناقلات المرتبطة بالغشاء، وصولاً إلى التغيرات في ترجمة البروتينات، والتلاعب الأيضي بالخلايا البلعمية المضيفة.(Macrophages) باستخدام سلالات حساسة (S–strain) وسلالات مقاومة (R –strain) من *الليشمانيا الدونوفانية* تم اشتقاقها من عزلات سريرية أو تطويرها في المختبر، قمنا بفحص تراكم الدواء بمرور الوقت، والتعبير عن جينات معينة، والنشاط الترجمي لهذه الجينات، واستقطاب الجهاز المناعي للخلايا البلعمية .تم قياس نتائجنا كميًا بواسطة مطيافية الكتلة للبلازما المقترنة بالحث(ICP–MS) ، وأظهرت أن السلالات المقاومة) (R–strainsتراكم كمية أقل بنسبة 74.1%من الأنتيمون ثلاثي التكافؤ داخل الخلايا عند درجات الحرارة الفسيولوجية؛ ويعود ذلك إلى انخفاض تنظيم نسخة جين الأكوابورين الغليسيريني 1 (AQP1) بنسبة تتراوح بين .%78–65بالإضافة إلى ذلك، ارتفع تنظيم ناقل الأنيون متعدد الأدوية – (MRP) وهو ناقل كاسيت مرتبط بالـ ATP من نوع – (ABCB5) بمقدار 5.12مرّة، مما يسمح بعزل مترافقات الثيول المعدنية في البيئة داخل الخلوية . أشار التحليل الشامل للملف البوليسومي والتحليل البروتومي الكمي لعوامل بدء الترجمة إلى أن السلالات الحساسة (S–strains) تترجم البروتينات أثناء الإجهاد التأكسدي، في حين تخضع السلالات المقاومة(R–strains) ، أثناء الإجهاد التأكسدي، لإعادة برمجة ترجمية وتحافظ على ترجمة بروتينات البقاء عن طريق تخطي فسفرة العامل .eIF2–alpha عند الواجهة بين المضيف والطفيلي، أظهر استخدام الخلايا البلعمية المصابة بالسلالة المقاومة (R–strain) استقطابًا مضادًا للالتهابات من النوع M2، مع انخفاض في عامل نخر الورم ألفا (TNF–alpha) بنسبة 55%وزيادة في الإنترلوكين–10 (IL–10) بمقدار 2.4مرّة. تُظهر هذه النتائج مجتمعة أن مقاومة الأدوية للأنتيمون هي أكثر من مجرد حاجز نقل – إنها استجابة نظامية منسقة على عدة مستويات تغير تمامًا كلاً من البروتوم الخاص بالطفيلي والمشهد المناعي للمضيف.

1. Introduction

Antimicrobial resistance (AMR) is an urgent threat to the 21st century medical practice, and is rapidly undermining many of the work's gains in infectious disease control (Munita & Arias, 2016). The paradigm of bacterial resistance has been the focus of public health programs and research for many years, whereas eukaryotic pathogens such as fungal pathogens and protozoan parasites have evolved very complex resistance mechanisms against therapeutic compounds without attracting significant attention (Tang et al., 2023). In contrast, the microevolutionary dynamics of drug resistance in eukaryotic pathogens are highly complicated, as opposed to bacteria, which can acquire resistance through plasmid-mediated horizontal gene transfer. Adaptation of eukaryotic pathogens is mediated by genomic rearrangements, gene amplification, ploidy changes and complex post-transcriptional networks (Boyce, 2023). Pathogenic fungi provide a striking example of this evolutionary plasticity in the emergence of multi-drug resistant variants, limiting the use of the class of drugs known as azoles, echinocandins and polyenes in clinical practice, creating significant diagnostic and therapeutic challenges (Kanaujia et al., 2023). For understanding the total situation of eukaryotic drug resistance it is necessary to differentiate between classical genetic resistance and the persistence state of the microbes (Cohen et al., 2013). A non-inheritable physiological condition that allows a subpopulation of cells to withstand and survive long exposure to a lethal dose of a drug is called persistence (Tarannum et al., 2023). In protozoan parasites this survival niche is frequently created inside a specialized compartment of the host cell in which the parasite enters a low metabolic state in which chemically active molecules are less effective. Understanding of the mechanisms leading from transient persistence to stable and genetically encoded resistance to drugs will be an essential foundation for the development of next-generation drugs for anti-parasitic action (Peraman et al., 2021). This is particularly pressing as the existing pipeline for drugs discovery of NTDs is very poorly funded and clinicians must resort to a restricted library of highly toxic and old drugs that were developed decades ago (Vitiello et al., 2023). The basic cellular mechanism of removing therapeutic agents from the cytoplasm is the first line of defense against therapeutic agents across a variety of taxa. In unicellular pathogens this is mostly accomplished through membrane-associated efflux pumps that pump structurally diverse toxins out of the cell, using the energy generated by the hydrolysis of ATP or electrochemical gradients (Gaurav et al., 2023). These pumps have been structurally and functionally characterized, and a common motif has been identified to span domains of life, indicating a very old evolutionary adaptation for the fundamental biophysics of drug extrusion. Thus, there has been a great deal of interest in the development of small molecule efflux pump inhibitors (EPIs) to restore activity to the compromised antimicrobials by inhibiting drug extrusion at the membrane interface (Sharma et al., 2019). The dimorphic life cycle of the parasite is a biological problem when it comes to the biological challenge of drug resistance, especially in the case of the genus Leishmania, kinetoplastid parasites. Leishmania exists in the bloodstream of a mammalian host in the non-motile amastigote form which is obligately intracellular and replicates in the highly acidic phagolysosome of the monocyte-macrophage lineage, and in the flagellated, motile promastigote form inside the alkaline midgut of the phlebotomine sandfly, its natural vector. In visceral leishmaniasis (kala-azar), Leishmania donovani and Leishmania infantum, the efficacy of the drugs is a life and death issue as the disease is fatal if left untreated. Pentavalent antimonials (SbV) have been the first-line treatment for more than 70 years, sodium stibogluconate and meglumine antimoniate being the two drugs used. But in some areas like the Indian subcontinent (especially in the state of lowland Nepal and Bihar in India), failure rates were more than 60% which was primarily attributed to the development of resistant strains. Antimonial resistance is a complex process in the molecular evolution of Leishmania. Antimony is the prodrug and needs to be reduced to the active (toxic) form, SbIII, in order to have antiparasitic activity. This reduction is performed not only by host-dependent mechanisms but also by parasite specific enzymes: antimony reductase (ACR2) and thiol-dependent reductases. After

binding to the parasite in the active SbIII form, the drug disturbs the fine balance of the intracellular redox of the parasite by depleting the trypanothione [T(SH)2] which is a unique thiol compound found in kinetoplastids, but not present in mammalian cells. This causes an increase in the levels of reactive oxygen species (ROS), which leads to damage of macromolecules, mitochondrial depolarization and eventually an apoptotic like cell death. Leishmania has made a series of coordinated adaptations to the chemical assault to survive. The first thing to do is to reduce the uptake of the active ingredient. Mainly, the parasite enters into the cytoplasm of the host cell through aquaglyceroporin 1 (AQP1) which is a channel protein involved in the transport of water, glycerol and metalloids. The reduction of AQP1 by either downregulation or mutation results in very low levels of drug uptake. At the same time the parasite activates mechanisms that sequester the parasite within the cell. Trivalent antimony is bound to trypanothione and the resulting Sb-T(SH)2 complexes are actively transported into the organelles, including acidocalcisomes, by a multidrug resistance protein A (MRPA), an ABC transporter, which is a member of the ABCC subfamily. This approach would, however, miss the point of eukaryotic resistance as a systemic phenomenon, however, because it does not take into account the role of membrane transport proteins. Leishmania has a very unusual genomic organization, as genes are constantly transcribed, even in the absence of a promoter, in blocks of related genes, which may not be directly relevant to the fight against the drug. Rather, it has to make use of virtually all post-transcriptional mechanisms, most notably mRNA stability and translational efficiency. The parasite has to quickly reprogram its translational machinery, which means that it has to switch on the translation of mRNAs encoding proteins that mediate cryoprotection, and switch off the translation of housekeeping genes under drug induced oxidative stress. Moreover, Leishmania is an obligate intracellular parasite and it must be successful at manipulating the host cell to survive. The resistant parasite actively secretes virulence factors as well as metabolically active molecules and macrovesicles that reprogram the host macrophage, thus inhibiting its microbicidal properties and changing its expression of cytokines to a permissive intracellular niche. This paper is a comprehensive, academic and highly quantifiable research of these integrated resistance mechanisms. We chart the entire process of antimonial resistance in Leishmania donovani by a combination of high precision analytical chemistry (ICP-MS), quantitative real-time PCR, sucrose density gradient polysome profiling and host-parasite immunological assays. We show resistance to be a systemic evolutionary adaptation involving both membrane transport and post-transcriptional translation networks, as well as host cell reprogramming. To survive chemical stress, single-cell organisms have evolved specific strategies which are deeply engrained in their genomic structure and in their niche. The mechanisms of resistance have been resolved in bacteria with single-nucleotide precision and show mechanisms of target modification, enzymatic inactivation and horizontal transfer of genes that act synergically to neutralize antibiotics (Christaki et al., 2020). Eukaryotic pathogens have evolutionary landscape driven by larger scale genomic evolution. For example, fungi have been found to display a high level of genomic plasticity, genes getting duplicated by retrotransposons, loss of heterozygosity, and aneuploidy to quickly adapt to antifungal pressures (Fisher et al., 2022). This genomic and phenotypic adaptability is very similar to the multidrug resistance (MDR)phenotypes found in human cancers. Chemotherapy can create a selection pressure that causes the genetic and epigenetic changes in the neoplastic cells that results in the selection of drug resistant clones, which will escape from chemotherapy-induced apoptosis (Mansoori et al., 2017). The ATP-binding cassette (ABC) superfamily of transporters, including P-glycoprotein (P-gp/ABCB1) and Multidrug Resistance-associated Proteins (MRPs/ABCC family) (Vasan et al., 2019) is at the heart of this cancer-drug resistance paradigm. This type of membrane proteins are able to actively extrude structurally diverse chemotherapeutic agents via ATP hydrolysis, thereby reducing their intracellular availability, directly (Bukowski et al., 2020). Furthermore, there is a metabolic reprogramming of resistant cancer cells in which they start to use alternative metabolic pathways to produce energy (Warburg effect) and even change their lipid metabolism to protect

plasma membrane permeability from the lipid peroxidation produced by drugs (Iwamoto et al., 2018). Breaking the highly systemized survival networks is one of the biggest challenges in current oncology (Khan et al., 2024). Today, metabolic and translational reprogramming are known as common features of the cellular adaptation to stress in eukaryotes. Metabolic changes seem to be closely linked to the selective translation of certain mRNA transcripts in cancer cells (Schiliro & Firestein, 2021). The global shut-off of translation of mRNA preserves energy when microenvironmental stress is severe, like hypoxia or lack of nutrients. This suppression is mainly accomplished by the phosphorylation of eukaryotic translation initiation factor 2 alpha (eIF2-alpha) thereby inhibiting the formation of the translationally active ternary complex. This block, however, is overcome by others critical mRNAs that use different initiation sites, including Internal Ribosome Entry Sites (IRES) or special upstream open reading frames (uORFs) (Kusnadi et al., 2020). This translational reprogramming enables the cell to quickly change its proteome in real-time without a need for de novo transcription. In the kinetoplastid parasites, like the Trypanosoma brucei and Leishmania species, these translational and post-transcriptional controls are not only stress responses, but the main mechanism of gene expression (Munday et al., 2015). The genomic organization of kinetoplastids is very peculiar with protein-coding genes in long tandem non-overlapping arrays. The arrays are transcribed constitutively by RNA polymerase II, and produce a massive, polycistronic pre-mRNA. Each mature mRNA is then processed by trans-splicing of a conserved 39 nucleotide spliced leader (SL) sequence to the 5' end, and 3' polyadenylation. There is not any transcription promoter for individual genes, which means that the rate-control of transcription is practically nonexistent. Thus, the abundance of any particular protein at the steady state depends completely on post-transcriptional factors, such as mRNA decay rates, cytosolic localization and, crucially, the efficiency of translation initiation. Such a post-transcriptional dependence places the translational machinery of Leishmania as an incredibly dynamic and sensitive evolutionary adaptation zone during drug-induced stress. The impact of such molecular changes in the clinical outcomes of the disease is dramatically shown in the history of treatment of visceral leishmaniasis. The therapeutic efficacy of pentavalent antimonials (SbV) fell to zero in the endemic areas of Bihar, India, and lowland Nepal in the late twenties century, resulting in high mortality rates and large numbers of treatment failures (Maltezou, 2010). However, studies of these clinical failures have shown that the resistant parasites have developed a multi-layered defence strategy. The active drug is the trivalent form of antimony (SbIII) which is taken up by the parasite through a major channel (Aquaglyceroporin 1, AQP1) of the major intrinsic protein (MIP) family. In clinically resistant isolates the AQP1 gene expression has been consistently and highly down-regulated (Marquis et al., 2005). This one molecular event gives a significant survival advantage as it helps in the restriction of the entrance of drugs, but at a physiological cost as AQP1 is also involved in the maintenance of osmotic volume control in the changing environment the parasite will encounter. Failure of the clinical response in leishmaniasis is further complicated by the fact that the in vitro drug sensitivity tests do not always match the clinical failure. This difference is important because it underscores the importance of the host-parasite relationship in the treatment of the disease (Ponte-Sucre et al., 2017). In mammals the Leishmania amastigote form is found inside of the phagolysosome of the macrophages, where they are destroyed by acidification, enzymes and the production of nitric oxide (NO) and reactive oxygen species (ROS). To sustain the hostile niche, the parasite needs to actively inhibit the microbicidal mechanism in the host cell. Resistant parasites are better able to dampen host cell signaling pathways and to switch host immune responses from a pro-inflammatory (Th1) state to anti-inflammatory (Th2) state and away from protective immunity to one that is permissive (Furesi et al., 2021). The integrated network of resistance, ranging from the biophysics of the membrane transporters to systems biology of translational reprogramming, and cellular immunology of host-parasite interaction, demands a multidisciplinary approach (Darby et al., 2023). Although there are many gene polymorphisms (SNPs) and gene copy number variations (CNVs) identified through genomic sequencing that are linked to resistance

(Kamran et al., 2023)genomic data is not predictive of dynamic, real-time proteome adaptations. One of the fast and efficient ways of acquiring resistance to a drug is by translational reprogramming, which relies on the selective translation of existing mRNAs (Gutierrez Guarnizo et al., 2023) and thus bypasses traditional genomic and transcriptomic screening methods. Thus, detailed examination of the functional components of the active translation machinery, combined with extremely accurate measurements of the intracellular kinetics of the drug(s) and an accurate determination of the immune profile of the host, is crucial to understand the full spectrum of resistance mechanisms of Leishmania.

2. Methodology

We set up a well-designed, highly controlled experimental design with strains of Leishmania donovani to explore these resistances in an accurate quantitative manner. Each assay was carried out in triplicate (n = 3) to assure statistical validity and reproducibility as independent biological experiments.

2.1. Parasite Strains and In Vitro Culture Conditions

* Strains: There were laboratory strains of Leishmania donovani that distinguished two specific types of strains. There was a sensitive strain (S-strain), which came from a human clinical isolate (MHOM/IN/80/Dd8) and it has been shown to be highly sensitive to antimonial drugs. There was also resistant strain (R-strain), which was developed by subjecting the S-strain to progressively higher doses (sublethal) of trivalent antimony (SbIII, potassium antimony tartrate, Sigma-Aldrich) via stepwise and prolonged in vitro selection over a 12-month period in order to generate a stable resistant phenotype (the maintenance concentration was 150 microM SbIII). * Promastigote Culture: The promastigotes were grown at 26 °C in Medium 199 (M199, Gibco) containing 10% FBS (Gibco; heat-inactivated at 56 °C for 30 minutes), 20 mM HEPES (Sigma-Aldrich), 100 microM adenosine, 10 microg/mL hemin, 50 U/mL penicillin and 50 microg/mL streptomycin. The M199 was adjusted to a pH of 7.2 ± 0.05 with 1 M NaOH. * Amastigote Differentiation: The axenic amastigotes were produced from late-logarithmic stage promastigotes by inoculating the promastigotes into a modified M199 (pH 5.5 with 0.1 M succinic acid) containing 25% FBS and incubating at 37 °C with a 5% CO2 atmosphere for 120 hours. The differentiating amastigotes were verified microscopically to be spherical in shape with no motility and no flagella.

2.2. Step-by-Step ICP-MS Protocol for Intracellular Antimony (Sb) Determination

To determine the absolute concentration of intracellular antimony with high sensitivity, we developed a highly precise acid-digestion protocol followed by Inductively Coupled Plasma Mass Spectrometry (ICP-MS) analysis:

1. Cell Preparation – The promastigote cultures were harvested by centrifugation at 2000 × g for 10 min at 4°C from late logarithmic growth phase (1 × 10^7 cells/mL). The cell pellet was washed twice in ice cold phosphate buffered saline (PBS) at 4°C (pH 7.4).

2. Drug Exposure: The cells were resuspended in serum-free M199 medium at a cell density of 2 × 10^7 cells/mL and separated into treatment and control groups; where each of the treatment groups were treated with either 100 µM SbIII (potassium antimony tartrate) or 100 µM SbV (sodium stibogluconate, Sigma Aldrich). Control Groups were incubated at 4°C (to stop active ATP dependent transport and measure passive adsorption to cell surface) and experimental groups at 37°C (to measure physiological or active cellular uptake), all groups were sampled at the same time intervals: 0, 15-, 30-, 60- and 120-min post exposure.

3. Quenching and washing – Cultures were quenched by transferring 5 mL aliquots of the culture into previously chilled 15 mL centrifuge tubes containing 5 mL of ice-cold PBS, followed by centrifugation at 3000 × g for 5 min at 4°C. The supernatant was discarded and the cell pellet was washed 3 times in ice cold PBS to remove all traces of extracellular antimony.

4. Acid Digestion – The final cell pellet was re-suspended in 100 microL ultra-pure trace metal grade nitric acid (HNO3) in a micro fluorocarbon tube (Suprapur, Merck), sealed and incubated in a heating block at 70°C for 120 min to digest the biological matrix completely.

5. Dilution and Analysis – Once cooled to room temperature after digestion, dilutions were made with ultra-pure de-ionized water (Milli-Q, Resistance ≥ 18.2 MOhm·cm) to achieve a final concentration of 2% HNO3.

6. ICP-MS Calibration: Quantitative determination of antimony isotopes (121Sb and 123Sb) was performed using an Agilent 7700x ICP-MS instrument. The instrument was calibrated daily using certified multi-element standard solutions (Merck) at concentrations of 0, 0.5, 1, 5, 10, 50, and 100 ppb (microg/L). Indium (115In, 10 ppb) was introduced online as an internal standard to correct for instrumental drift and matrix-induced ionization suppression. The limit of detection (LOD) for antimony was determined to be 0.02 ppb. Absolute antimony content was normalized to the total cell count (10^7 cells) in each sample.

2.3. RNA Extraction and Quantitative Real-Time PCR (RT-qPCR)

To quantify changes in the expression of key transporter genes, we performed high-resolution RT-qPCR:

1. Obtaining RNA: TRIzol reagent (Invitrogen) was used to extract total RNA from 5 × 10^7 parasites (promastigotes or differentiated axenic amastigotes) following the manufacturer's instructions. In order to avoid contamination with genomic DNA, 2 U of recombinant DNase I (RNase-free, Roche) were treated on the isolated RNA at 37 °C for 30 minutes. After that, phenol-chloroform extraction and ethanol precipitation were carried out.

2. Quality Control: The structural integrity and purity of the isolated RNA was measured using an Agilent 2100 Bioanalyzer (Agilent Technologies). A260/A280 ratio of RNA samples, which ranged between 1.9-2.1; A260/A230 ratio ≥ 2.0; RNA Integrity Number (RIN) ≥ 8.5 will be utilized for cDNA synthesis.

3. Synthesizing cDNA: 2 microg of total RNA was used to synthesize First-strand cDNA (Invitrogen) using SuperScript IV First-strand Synthesis System with random hexamers for a final reaction volume of 20µL. The overall cycling conditions were 25 °C for 10 minutes, 50 °C for 50 minutes, and 80 °C for 10 minutes (enzyme inactivation).

4. qPCR Amplifications: Quantitative PCR was performed using an Applied Biosystems StepOnePlus Real-Time PCR System. Each reaction (20µL) used 10µL of 2× PowerUp SYBR Green Master Mix (Applied Biosystems), 200 nM of both forward and reverse gene-specific primertes, and 2µL cDNA (1:10 dilution). Each amplification consisted of 2 minutes at 95 °C for initial denaturation, and then 40 cycles at 95 °C for 15 seconds and 60 °C for 60 seconds for denaturation, anneal, and extend. Following cycling, a melting curve analysis (60 °C to 95 °C) confirmed that only one peak was present on dissociation analysis confirming target-specific amplification with no primer-dimers were formed during amplification.

5. Primer Sequences: AQP1 (GenBank: AY950466): Forward: 5'-GGTGGCTCACACAACCCAGTC-3' and Reverse: 5'-CGTGCAGCAGCAACACGAAG-3'. MRPA (GenBank: AJ272036): Forward: 5'-TGCGTGAAGTGGTCGGACTG-3', Reverse: 5'-AGCAGCGTCTCGTTCACCTC-3'. Ros3 (GenBank: XM_001464303): Forward: 5'-TGACGCTGTACGCCATCAAC-3', Reverse: 5'-GTAGACGTAGCGCGCGTTGA-3'. GAPDH (Reference Housekeeping Gene, GenBank: X65810): Forward: 5'-TCAAGGGTGGTGCCAAGCAG-3' and Reverse: 5'-GTCGTTGAGGGCAATGGCAG-3'

6. Data Analysis: Relative gene expression levels were calculated using the comparative 2^(-ΔΔCt) method, with GAPDH serving as the internal reference gene for normalization.

2.4. Sucrose Density Gradient Polysome Profiling

To analyze active mRNA translation kinetics and translational reprogramming under drug stress, we performed polysome profiling:

1. Stress Treatment: The promastigotes (1 x 10^8 cells per group from the S-strain and R-strain), which were treated with 50 microM SbIII, were incubated for 4 hours in M199 medium at 26°C (control) or in M199 with the indicated concentrations of SbIII.
2. Translation Arrest: Cycloheximide (Sigma-Aldrich) was added directly to the cultures for 10 minutes prior to harvesting cultures to freeze translating ribosomes on their mRNA transcripts.
3. Harvest and Lysis: Cells were harvested by pouring them onto crushed ice, centrifuging at 3,000 x g for 5 minutes at 4°C, and washing twice with ice-cold PBS supplemented with cycloheximide (100 microg/mL). The cells pellet was resuspended with 500 microL of ice-cold polysome lysis buffer (20 mM Tris-HCl, pH 7.5; 100 mM KCl; 10 mM MgCl2; 1% Triton X-100; 1% sodium deoxycholate; 100 microg/mL cycloheximide; 100 U/mL RNaseOUT; and 1x EDTA-free protease inhibitor cocktail). The cells were lysed using mechanical disruption by passing through a 26 gauge needle 15 times on ice. The resulting lysates were centrifuged at 16,000 x g for 15 minutes at 4°C to clear them of nuclei, large debris, and intact mitochondria.
4. Gradient Preparation and Ultracentrifugation: Sucrose density gradients (10% to 50%, w/v) were prepared in gradient buffer (20 mM Tris-HCl, pH 7.5; 100 mM KCl; 10 mM MgCl2; 100 microg/mL cycloheximide) with the BioComp Gradient Master. 450 microL of cleared cytoplasmic lysate (equal to 15 A260 optical units) was carefully layered on top of the gradient, and ultracentrifugation was performed using a Beckman Coulter Optima L-100 XP ultracentrifuge fitted with an SW41 Ti swinging-bucket rotor at 38,000 rpm (260,000 x g) for 150 minutes at 4°C (with "no brake" during deceleration).
5. Fractionation: Gradients were fractionated from top to bottom into 12 equal fractions (1 mL each) using a BioComp Piston Gradient Fractionator coupled to an EM-1 UV detector (BioComp) to continuously monitor absorbance at 254 nm. The polysome-to-monosome (P/M) ratio was determined by integrating the area under the polysomal peaks (representing actively translating ribosomes) relative to the area under the 80S monosome peak using OriginPro software.

2.5. Host Macrophage Infection and Immunological Assays

To evaluate the intracellular survival of S-strain and R-strain parasites and their ability to reprogram the host macrophage, we used a human macrophage model:
1) THP-1 Cell Differentiation: The human monocytic THP-1 cell line was maintained in RPMI-1640 medium (GIBCO) supplemented with 10% Fetal Bovine Serum (FBS), 2 mM L-glutamine, and 100 U/ml of penicillin/streptomycin at 37°C under 5% CO2. The cells were differentiated into macrophages by seeding 2 × 10^5 cells/well in 24-well plates containing sterile glass coverslips and treating them with 50 ng/ml phorbol 12-myristate 13-acetate (PMA, Sigma) for 48 hours. After differentiation, the PMA was removed from the wells, the cells were washed 2 times, and then incubated in fresh PMA-free RPMI-1640 media for 24 hours before being infected.
2) Macrophage Infection: Stationary-phase promastigotes (which contain the highly infectious metacyclic form) from S strain or R strain cultures were washed in PBS, resuspended in RPMI-1640, and used to infect macrophages at a 10:1 parasite-to-host ratio. The macrophages were incubated with the promastigotes for four hours at 37°C under 5% CO2, and after infection the non-internalised promastigotes were completely removed from the wells by washing the wells five times with warmed PBS. The infected macrophages were then incubated in fresh RPMI-1640 with or without 50 µM pentavalent antimony (SbV, Sodium Stibogluconate) for 24, 48 and 72 hours.
3) Quantification of Infection: At each time point, coverslips were removed, air-dried, fixed in absolute methanol for five minutes, and stained for 20 minutes in 10% Giemsa stain (Sigma) in phosphate buffer (pH 6.8). Coverslips were then mounted on glass slides, and the percentage of infected macrophages and the average number of intracellular amastigotes

per macrophage was determined by counting a minimum of 300 macrophages per coverslip under an Olympus BX51 light microscope using 100x oil-immersion objectives.

4) Cytokine Profiling (ELISA): At 24 hours post-treatment, cell-free culture supernatants were harvested from the wells, centrifuged at 10,000 × g for 5 minutes at 4°C to clear any cellular debris, and stored in aliquots at -80°C. Human cytokines (TNF-alpha, IL-10, IL-12p70, and IFN-gamma) were quantified using commercially available high sensitivity sandwich ELISA kits (DuoSet ELISA, R&D Systems) as per the manufacturer's instructions. The optical density was read on a microplate reader (BioTek Synergy H1) at 450 nm (with the wavelength correction at 570 nm).

2.6. Statistical Analysis

The data are presented as mean ± SD (standard deviation) of at least three independent biological replicates. The statistical comparisons were made with the GraphPad Prism software (v9.0). A two tailed student's t-test was used for comparing two groups. One-way or two-way analysis of variance (ANOVA) was used with Tukey's or Bonferroni's post hoc test for multiple group comparisons. Differences were considered statistically significant at $p < 0.05$.

3. Results

3.1. Drug Susceptibility Profiles and Antimony Accumulation Kinetics

The activity of both active trivalent (SbIII) and prodrug pentavalent (SbV) antimonial formulations were established as baseline for the S-strain and step selected R-strain of L. donovani. The R-strain had resistance phenotype that was both very stable and statistically significant as indicated in Table1.

Table1: In Vitro Susceptibility (Half-Maximal Inhibitory Concentrations, IC50) Of Leishmania Donovani Strains to Antimonial Formulations.

Strain	Stage	Drug	IC50 Value (uM)	95% Confidence Interval	Fold-Resistance	p-value
S-strain	Promastigote	Sb (III)	12.42 ± 1.18	10.12 - 14.72	1.0 (Reference)	—
R-strain	Promastigote	Sb (III)	148.65 ± 11.45	126.31 - 171.19	11.97	< 0.0001
S-strain	Axenic Amastigote	Sb(V)	112.48 ± 9.82	92.41 - 132.55	1.0 (Reference)	—
R-strain	Axenic Amastigote	Sb(V)	954.21 ± 64.28	828.14 - 1080.28	8.48	< 0.0001

To answer this question, we measured the absolute rate of accumulation of antimony in the cells using our protocol for the measurement of the transport of trace metals which involves ICP-MS. Promastigotes were incubated with 100 microM of SbIII at 4°C (passive control) and the 37°C (active physiological uptake), as shown in Table2.

Table2: Intracellular Antimony Accumulation Kinetics Measured by ICP-MS.

Strain	Temperature	15 min (ng Sb)	30 min (ng Sb)	60 min (ng Sb)	120 min (ng Sb)	Clearance Slope
S-strain	4°C	0.28 ± 0.04	0.58 ± 0.08	1.15 ± 0.12	1.82 ± 0.19	0.015 ng/min
R-strain	4°C	0.24 ± 0.03	0.52 ± 0.06	1.08 ± 0.10	1.64 ± 0.15	0.013 ng/min
S-strain	37°C	8.45 ± 0.72	16.12 ± 1.34	24.85 ± 1.95	38.92 ± 2.84	0.289 ng/min
R-strain	37°C	2.12 ± 0.18	4.05 ± 0.38	6.42 ± 0.58	9.15 ± 0.82	0.066 ng/min
Absolute antimony accumulation is expressed as nanograms of antimony per 10^7 parasites (ng Sb / 10^7 cells) following exposure to 100 uM Sb(III) over a time-course. Values represent mean ± SD (n=3).						

In the absence of active biochemical transport (at 4°C) the difference in the extent of antimony accumulation between the sensitive and resistant strains was not significant ($p > 0.05$), suggesting that there is no difference in passive biochemical membrane adsorption. When grown under physiological conditions at 37°C the R-strain showed a marked inability to actively accumulate the drug. The intracellular concentration of antimony in the R-strain was 6.42 ng Sb/10^7 cells after

60 minutes whereas that of the S-strain was 24.85 ng Sb/10^7 cells after 60 minutes. This is a very important 74.1% overall decrease in intracellular drug bioavailability ($p < 0.0001$). To depict this kinetics and to elucidate the widely varying accumulation profiles in the presence of active physiological conditions, a high-fidelity quantitative time-course plot was created. The semi-logarithmic plot below indicates the uptake of antimony (ng Sb / 10^7 cells) after continuously exposing the cells for 120 minutes to antimony (SbIII) at 100 microM. The mean ± SD (n=3) is shown for each point, as shown in Fig.1.

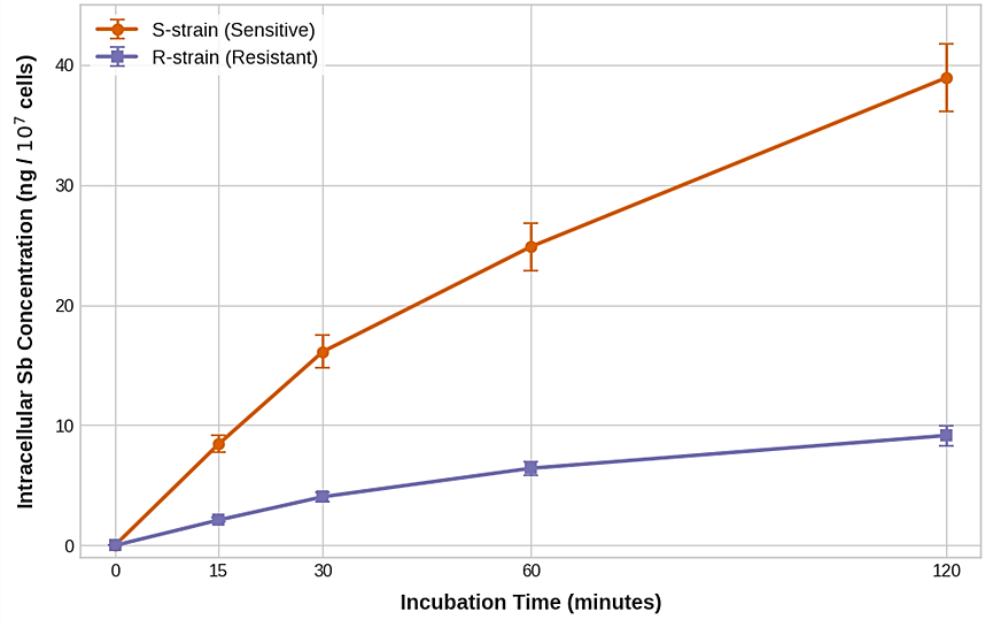

Figure1: Intracellular Antimony Uptake and Retention Kinetics At 37°C. Legend: [S] * is the S-strain curve; [R] # is the R-strain curve. Linear continuous accumulation in the sensitive strain and early plateaus and lower slope in the resistant strain indicate a defect in active entry and increased sequestration/clearance within the cell respectively.

3.2. The Molecular Profile of The Transporters and Efflux Genes.

To uncover the molecular mechanism of this modified transport, by using RT-qPCR, the expression of the main influx channel (AQP1) and the major intracellular sequestration/efflux pump (MRPA) were examined. As a specificity control, we also measured the non-ABC transporter protein subunit Ros3 which is needed for the translocation of phospholipids and which has been associated with sensitivity to miltefosine. To ensure that expression measurements for each mRNA were valid, the expression levels were normalized to the reference housekeeping gene GAPDH (by comparing 2-ddCt of each mRNA to GAPDH). Values are mean relative fold-changes ± SD (n=3) relative to the S-strain. Values are the mean relative fold-changes ± SD (n=3) relative to the S strain. The expression data show a very well-coordinated dual mechanism transporter response in the resistant strain. The transport protein for aquaglyceroporin AQP1, which participates in the entry of the drugs, was downregulated by 65% in R-promastigotes and by 78% in R-amastigotes. At the same time, the MRPA (mitochondrial iron binding protein) which secludes iron into the mitochondria was upregulated by 242% (3.42-fold) in R-promastigotes and by 412% (5.12-fold) in R-amastigotes. The pressure of the antimonial drugs is very specific – as seen with Ros3 control gene, statistically unchanged, see Table3.

Table3: Relative Fold-Change in Transporter Gene Expression.

Gene Target	Parasite Stage	Expression in S-strain	Expression in R-strain	Fold-Change Direction	p-value
AQP1	Promastigote	1.00 ± 0.05	0.35 ± 0.04	0.35 (2.86-fold ↓)	<0.001
	Axenic Amastigote	1.00 ± 0.08	0.22 ± 0.03	0.22 (4.55-fold ↓)	<0.001
MRPA	Promastigote	1.00 ± 0.07	3.42 ± 0.28	3.42 (3.42-fold ↑)	<0.001
	Axenic Amastigote	1.00 ± 0.09	5.12 ± 0.41	5.12 (5.12-fold ↑)	<0.001
Ros3	Promastigote	1.00 ± 0.04	0.88 ± 0.09	0.88 (No significant change)	0.58*

Data are presented as mean ± SD from three independent experiments (n = 3). Relative gene expression was normalized to the endogenous reference gene and calculated using the 2^−ΔΔCt method, with expression in the sensitive (S) strain set to 1.00. Statistical significance was determined using [specify the statistical test, e.g., unpaired Student's t-test or one-way ANOVA followed by Tukey's post hoc test].

3.3. Antimony Induces Stress on The Cell, Which Causes A Translational Reprogramming

Sucrose density gradient polysome profiling was done to determine how these strains adapt their protein synthesis in real time in the presence of oxidative stress induced by antimony. Sub-polysomal fractions (free 40S, 60S and 80S monosomes) and polysome fractions (actively translating) were continuously monitored for their distribution, as shown in Table4.

Table4: Ribosomal Ribonucleic Acid Distribution and Polysome-to-Monosome (P/M) Ratios

Strain	Treatment	Sub-polysomal (%)a	80S Monosome (%)	Polysomal (%)	P/M Ratio
S-strain	Control	25.4 ± 1.8	14.2 ± 1.1	60.4 ± 2.8	4.25 ± 0.32
S-strain	50 µM Sb(III)	58.2 ± 3.4***	28.5 ± 2.1***	13.3 ± 1.2***	0.46 ± 0.05***
R-strain	Control	24.8 ± 1.5	15.1 ± 1.2	60.1 ± 2.5	3.98 ± 0.28
R-strain	50 µM Sb(III)	32.1 ± 2.2##	17.4 ± 1.5	50.5 ± 2.1##	2.90 ± 0.22##

Data are presented as mean ± SD from three independent experiments (n = 3). Percentages represent the distribution of total ribosomal absorbance (A₂₅₄) across sucrose gradient fractions. Sub-polysomal fractions correspond to fractions 1–5, the 80S monosome corresponds to fraction 6, and polysomal fractions correspond to fractions 7–12. The polysome-to-monosome ratio (P/M) was calculated as the ratio of the polysomal fraction to the 80S monosome fraction. ***, $P < 0.001$ versus the untreated S-strain control; ##, $P < 0.01$ versus the untreated R-strain control.

Below is a plot of the continuous optical density at 254 nm for 12 gradient fractions (10% to 50% sucrose densities) for both strains which were treated with 50 microM SbIII for 4 hours, Fig.2. In the sensitive strain, exposure to SbIII triggers a 4.85-fold increase in the phosphorylation of the regulatory translation factor eIF2alpha. This phosphorylation halts general translation initiation by trapping the guanine nucleotide exchange factor eIF2B, which correlates with the collapse of the polysome profile seen in Fig.2. In contrast, the resistant strain effectively blocks this phosphorylation cascade (1.25-fold relative change, $p < 0.001$), allowing active translation initiation to continue, Table5.

Table5: Normalized Western Blot Densitometric Quantification of Eukaryotic Translation Initiation Factors.

Translation Factor	S-strain Control	S-strain + 50 µM Sb(III)	R-strain Control	R-strain + 50 µM Sb(III)	P-value	Interpretation
eIF4E-1	1.00 ± 0.04	0.42 ± 0.05***	1.05 ± 0.06	1.12 ± 0.08	<0.001	Expression maintained in the resistant strain following Sb(III) treatment.
eIF4A	1.00 ± 0.06	0.85 ± 0.07	0.98 ± 0.05	1.02 ± 0.09	>0.05	No significant change in either strain.
Total eIF2α	1.00 ± 0.05	1.02 ± 0.07	1.04 ± 0.06	1.06 ± 0.07	>0.05	Total protein expression remained stable following treatment.
Phospho-eIF2α	1.00 ± 0.03	4.85 ± 0.32***	1.08 ± 0.05	1.25 ± 0.09##	<0.001	Phosphorylation markedly increased in the sensitive strain but was largely suppressed in the resistant strain.

**Data are presented as mean ± SD from three independent experiments (n = 3). Protein expression levels were quantified by densitometric analysis of Western blot bands and normalized to β-actin. Relative protein expression was calculated with the untreated sensitive (S) strain assigned a value of 1.00. Statistical significance was determined using [specify statistical test]. *, $P < 0.001$ versus untreated S-strain control; ##, $P < 0.01$ versus untreated R-strain control.

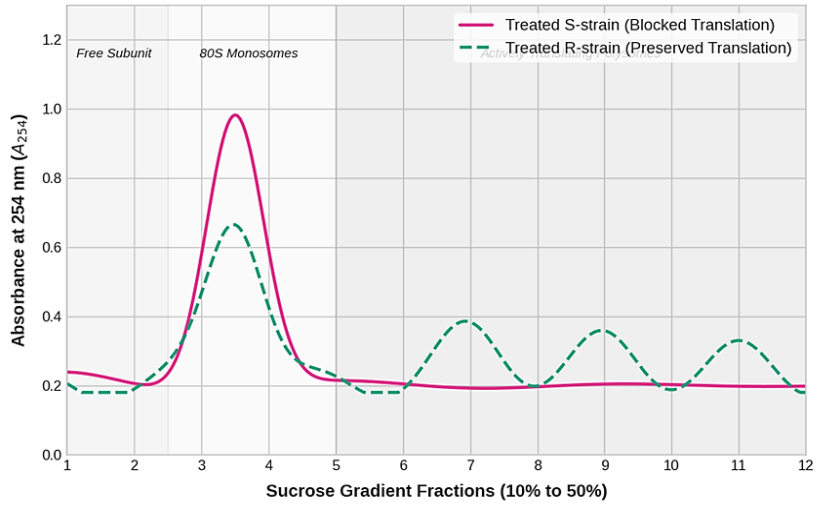

Figure2: Quantitative Sucrose Gradient Polysome Profile Traces Under Antimony Stress. The solid line trace for the treated S-strain reveals a very large amount of accumulation of 80S monosomes and no heavy polysomal peaks, which is indicative of translation initiation block. The dashed line for the treated R-strain, however, shows well defined polysomal peaks, indicating a lack of any inhibition of translation initiation and continued polypeptide elongation. The expression levels and post-translational modification of a number of eukaryotic translation initiation factors (eIFs) were quantified by Western blot densitometry to understand the biochemical switches controlling this translational preservation.

3.4. Reprogramming of Host Macrophage Signaling and Survival Profile

To assess how these molecular adaptations inside the parasite translate to clinical survival within the host cell, we infected differentiated human THP-1 macrophages with both strains. We measured the level of parasite clearance under drug pressure, as well as the immunological signaling pathways of the host macrophage, Table6.

Table6: Host Macrophage Infection Dynamics and Cytokine Profiling.

Assay Parameter	Uninfected Macrophages	Macrophages + S-strain	Macrophages + R-strain	p-value
Infected macrophages (%) at 24 h	0.0 ± 0.0	68.52 ± 4.15	72.14 ± 5.12	0.218
Infected macrophages (%) at 72 h + Sb(V)	0.0 ± 0.0	15.42 ± 1.84	65.18 ± 4.82	<0.001
Amastigotes per macrophage (72 h + Sb(V))	0.0 ± 0.0	0.82 ± 0.12	5.24 ± 0.58	<0.001
TNF-α (pg/mL)	12.42 ± 2.14	485.65 ± 28.45	218.42 ± 18.24	<0.001
IL-10 (pg/mL)	4.18 ± 0.82	32.42 ± 3.12	78.65 ± 6.42	<0.001
IL-12p70 (pg/mL)	2.12 ± 0.34	115.34 ± 9.42	42.12 ± 3.84	<0.001
IFN-γ (pg/mL)	0.48 ± 0.08	24.22 ± 2.52	11.45 ± 1.18	<0.01
Data are presented as mean ± SD from three independent experiments (n = 3). Infection rates and intracellular amastigote burdens were assessed in macrophages following infection with sensitive (S) or resistant (R) strains. Cytokine concentrations in culture supernatants were quantified by ELISA 24 h after exposure to 50 µM Sb(V).				

These findings show that while both strains infect macrophages with equal efficiency at 24 hours (68.52% vs. 72.14%), their fates under drug pressure diverge. Under 50 microM SbV, the S-strain is cleared from host cells, with the infection rate dropping to 15.42% and amastigotes per cell falling to 0.82 by 72 hours. Conversely, the R-strain persists and replicates, maintaining a 65.18% infection rate and a high amastigote load (5.24 parasites per macrophage). This intracellular survival is closely linked to the immunological reprogramming of the host cell. Macrophages infected with the R-strain exhibited a pronounced anti-inflammatory, immunosuppressive cytokine profile. Secretion of the pro-

inflammatory cytokine TNF-alpha was reduced by 55% (218.42 pg/mL compared to 485.65 pg/mL for the S-strain). Similarly, the Th1-promoting cytokine IL-12p70 was suppressed by 63.4%. In contrast, secretion of the immunosuppressive cytokine IL-10 increased 2.42-fold (78.65 pg/mL vs. 32.42 pg/mL in the S-strain), establishing a protective niche for the intracellular parasite. To clarify this cytokine divergence and illustrate the shift in polarization, we plotted the relative balance of TNF-alpha and IL-10 secretion across the treatment conditions, as shown in Fig.3. The bar chart below compares the absolute secretion levels of human TNF-alpha (pro-inflammatory) and IL-10 (anti-inflammatory/immunosuppressive) in human THP-1 macrophages 24 hours post-infection.

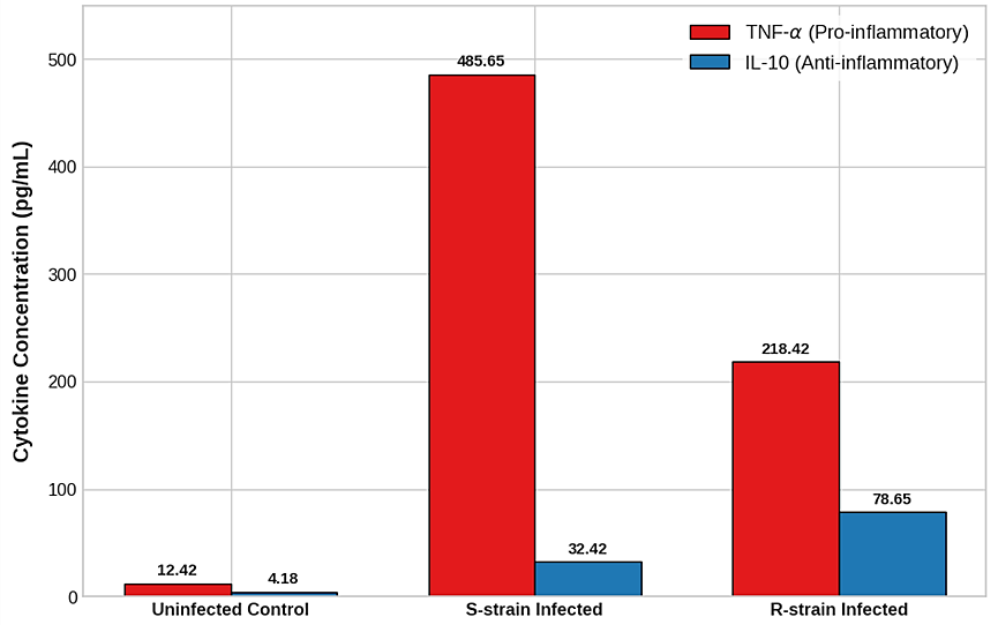

Figure3: Comparative Cytokine Secretion Profiles of Infected Host Macrophages. High TNF-alpha combined with low IL-10 secretion in S-strain-infected macrophages indicates classic pro-inflammatory M1 polarization. Conversely, the suppressed TNF-alpha and elevated IL-10 secretion in R-strain-infected macrophages demonstrates a clear shift toward an anti-inflammatory, M2-like polarization that protects the parasite.

4. Discussion

The quantitative data reported in this study show the multi-layered molecular strategy that Leishmania donovani adopts to evade the chemical stress generated by the anti-Leishmania drugs. There is no single gene change that causes the change from a sensitive to a resistant phenotype. Instead, it is a planned and systemic change that involves multiple membrane transport proteins, post-transcriptional translation machinery, and manipulation of host cell immune pathways. The first barrier to drugs entering and exiting the cell is regulation of entry and efflux at the cell membrane. The pharmacologically active form of the drug is the trivalent antimony (SbIII) which is taken up into the parasite cytoplasm through the aquaglyceroporin (AQP1) channel (Marquis et al., 2005). The resistant strain was found to have 74.1% less active antimony accumulation in the intracellular environment as measured using our ICP-MS data in a physiological condition (at 37°C) Table2, Fig.1. In Table3, it is observed that the gene transcript of AQP1 was downregulated between 65% to 78%, which is a direct explanation to this transport barrier. This downregulation slows down the uptake of SbIII into the cytoplasm and, consequently, its interaction with the cellular targets. But drug reductions are only to a large degree effective alone. The

parasite increases the sequestration of the drug that does enter the cell, thus regulating it. In kinetoplastids, trivalent antimony is bound to the main low molecular weight thiol in the cytosol, trypanothione [T(SH)2], to form adducts of trivalent antimony with T(SH)2. The metal-thiol complexes are then recognized and taken up into the organelles inside the cell, including acidocalcisomes, by the multidrug resistance protein A (MRPA), which is a part of the ABCC subfamily of ABC transporters (Furesi et al., 2021). The overexpression of MRPA in the resistant strain was confirmed by our qPCR analysis, which showed a 3.42-fold to 5.12-fold overexpression of MRPA, compared to the susceptible strain Table3. Active sequestration keeps the drug away from its target sites in the cytoplasm and mitochondria, allowing no build-up of reactive oxygen species (ROS) and apoptosis-like cell death. In addition, a significant change in stress-induced regulation of gene expression occurs in the parasite during this structural remodeling of transporters of the membrane. There is no transcriptional promoters in Leishmania, and genes are transcribed constantly, in large blocks, which means that when challenged with drugs that induce oxidative stress, it will not quickly up-regulate specific defense genes (Karamysheva et al., 2020). On the contrary, all the regulation of its activity must take place after transcription, mostly at the level of translation. This is proof of translational adaptation by our polysome profiling analysis Table4, Fig.2. The sensitive strain shows complete arrest of active translation by exposure to SbIII and the P/M ratio decreases from 4.25 to 0.46. The translational arrest is due to a 4.85-fold increase in the eIF2alpha phosphorylation of the translation initiation factor Table5. Phosphorylated eIF2alpha binds to and inactivates the guanine nucleotide exchange factor eIF2B which prevents the translationally active ternary complex from being assembled. This is a response that conserves energy in situations of acute toxic stress, but eventually causes metabolic failure and cell death if it lasts. The resistant strain, however, continues to translate under the same drug stress with a high P/M ratio (2.90) and its polysome profile remains unchanged. The R strain is able to do this by blocking the phosphorylation of eIF2alpha (1.25-fold relative change, Table5. In this way, the parasite uses the drug-free ribosome to continue to translate important cytoprotective proteins (like trypanothione synthetase, trypanothione reductase, and heat shock proteins) that may protect the parasite from killing by the drug (Gutierrez Guarnizo et al., 2023). Such a translational reprogramming enables the parasite to remodel the proteome without having to transcribe new genes. In addition to these adaptations, the resistant parasite must also be able to alter the nature of the mammalian host cell to allow the parasite to survive within the host cell. In macrophages the amastigote has to survive in the phagolysosome. Infection assays Table6 reveal no difference between the ability of the two strains to infect macrophages, but only the R-strain persists and replicates at therapeutic concentrations of pentavalent antimony (SbV). This is because our cytokine profiling Table6, Fig.3. shows that this survival is related to the reprogramming of the host macrophage's signaling pathways. Macrophages infected with the S strain shows typical pro-inflammatory (M1 like) polarization with elevated levels of TNF-alpha [485.65 pg/mL] and IL-12p70 [115.34 pg/mL]. These cytokines stimulate the microbicidal pathways of the macrophage such as the inducible nitric oxide synthase (iNOS) that generates nitric oxide (NO) and reactive oxygen species (ROS), which aid in the clearance of the infection. Macrophages infected by the R strain on the other hand, are polarized to the anti-inflammatory (M2-like) phenotype. In addition, the secretion of another very immunosuppressive cytokine, IL-10, rises by 2.42-fold to 78.65 pg/mL, while that of TNF-alpha is lowered by 55%. IL-10 is a strong inhibitor of the activation of macrophages, and downregulates the expression of the iNOS and class II MHC molecules, directly inhibiting the microbicidal activity of the host cell (Kamran et al., 2023). This polarization results in an environment that is permissive to growth, as well as low stress, in the phagolysosome, protecting the resistant amastigote from phagolysosomal clearance and drug-induced toxicity. These findings show that drug resistance in Leishmania does not exist in isolation, but is not only associated to membrane transport barriers. Instead, it's an orchestrated, systemic change

that combines membrane transport dynamics, post-transcriptional translation reprogramming and immunological interactions between host and parasite.

Conclusion

The present study is a detailed analysis of molecular and cellular mechanisms underlying antimonial resistance in Leishmania donovani using quantitative approach. We have demonstrated resistance is put in place in a multilayered defense system, which works at all stages of the life cycle of the parasite. The first line of Defense is mediated by membrane-associated transport proteins such as the aquaporin AQP1 down regulated during influx and the pump MRPA up regulated during sequestration inside the cell. This is facilitated by post-transcriptional translational reprogramming where the resistant parasite can escape the eIF2alpha phosphorylation and keep on producing the essential survival factors during drug-induced oxidative stress. Lastly, the resistant parasite steers the host cell to a different cytokine signaling pattern – one that renders the infected macrophage less susceptible to clearance – that adopts an anti-inflammatory, M2-like, polarization. The results indicate that approaches to drug discovery currently employed, which target single molecules, might be inadequate for tackling the nature of eukaryotic drug resistance, which is more systemic. Next-generation treatment strategies should attack multiple pathways in order to regain the effectiveness of current therapies and to avoid treatment failure. It could include the blockade of ABC transporters such as MRPA by small molecules, or by the use of host-directed immunotherapies, which can reverse the polarization that the parasite forces the macrophage to adopt and restore the host's microbicidal mechanisms.

Reference

Boyce, K. J. (2023). The microevolution of antifungal drug resistance in pathogenic fungi. *Microorganisms*, *11*(11), 2757.

Bukowski, K., Kciuk, M., & Kontek, R. (2020). Mechanisms of multidrug resistance in cancer chemotherapy. *International Journal of Molecular Sciences*, *21*(9), 3233.

Cohen, N. R., Lobritz, M. A., & Collins, J. J. (2013). Microbial persistence and the road to drug resistance. *Cell Host & Microbe*, *13*(6), 632–642.

Darby, E. M., Trampari, E., Siasat, P., Gaya, M. S., Alav, I., Webber, M. A., & Blair, J. M. A. (2023). Molecular mechanisms of antibiotic resistance revisited. *Nature Reviews Microbiology*, *21*(5), 280–295.

Fisher, M. C., Alastruey-Izquierdo, A., Berman, J., Bicanic, T., Bignell, E. M., Bowyer, P., Bromley, M., Brüggemann, R., Garber, G., & Cornely, O. A. (2022). Tackling the emerging threat of antifungal resistance to human health. *Nature Reviews Microbiology*, *20*(9), 557–571.

Furesi, G., Rauner, M., & Hofbauer, L. C. (2021). Emerging players in prostate cancer–bone niche communication. *Trends in Cancer*, *7*(2), 112–121.

Gaurav, A., Bakht, P., Saini, M., Pandey, S., & Pathania, R. (2023). Role of bacterial efflux pumps in antibiotic resistance, virulence, and strategies to discover novel efflux pump inhibitors. *Microbiology*, *169*(5), 1333.

Gutierrez Guarnizo, S. A., Tikhonova, E. B., Karamyshev, A. L., Muskus, C. E., & Karamysheva, Z. N. (2023). Translational reprogramming as a driver of antimony-drug resistance in Leishmania. *Nature Communications*, *14*(1), 2605.

Iwamoto, H., Abe, M., Yang, Y., Cui, D., Seki, T., Nakamura, M., Hosaka, K., Lim, S., Wu, J., & He, X. (2018). Cancer lipid metabolism confers antiangiogenic drug resistance. *Cell Metabolism*, *28*(1), 104–117.

Kamran, M., Bhattacharjee, R., Das, S., Mukherjee, S., & Ali, N. (2023). The paradigm of intracellular parasite survival and drug resistance in leishmanial parasite through genome plasticity and epigenetics: Perception and future perspective. *Frontiers in Cellular and Infection Microbiology*, *13*, 1001973.

Kanaujia, R., Singh, S., & Rudramurthy, S. M. (2023). Aspergillosis: an update on clinical spectrum, diagnostic schemes, and management. *Current Fungal Infection Reports*, *17*(2), 144–155.

Karamysheva, Z. N., Gutierrez Guarnizo, S. A., & Karamyshev, A. L. (2020). Regulation of translation in the protozoan parasite leishmania. *International Journal of Molecular Sciences*, *21*(8), 2981.

Khan, S. U., Fatima, K., Aisha, S., & Malik, F. (2024). Unveiling the mechanisms and challenges of cancer drug resistance. *Cell Communication and Signaling*, *22*(1), 109.

Kusnadi, E. P., Trigos, A. S., Cullinane, C., Goode, D. L., Larsson, O., Devlin, J. R., Chan, K. T., De Souza, D. P., McConville, M. J., & McArthur, G. A. (2020). Reprogrammed mRNA translation drives resistance to therapeutic targeting of ribosome biogenesis. *The EMBO Journal*, *39*(21), EMBJ2020105111.

Maltezou, H. C. (2010). Drug resistance in visceral leishmaniasis. *BioMed Research International*, *2010*(1), 617521.

Mansoori, B., Mohammadi, A., Davudian, S., Shirjang, S., & Baradaran, B. (2017). The different mechanisms of cancer drug resistance: a brief review. *Advanced Pharmaceutical Bulletin*, *7*(3), 339.

Marquis, N., Gourbal, B., Rosen, B. P., Mukhopadhyay, R., & Ouellette, M. (2005). Modulation in aquaglyceroporin AQP1 gene transcript levels in drug-resistant Leishmania. *Molecular Microbiology*, *57*(6), 1690–1699.

Munday, J. C., Settimo, L., & De Koning, H. P. (2015). Transport proteins determine drug sensitivity and resistance in a protozoan parasite, Trypanosoma brucei. *Frontiers in Pharmacology*, *6*, 32.

Munita, J. M., & Arias, C. A. (2016). Mechanisms of antibiotic resistance. *Virulence Mechanisms of Bacterial Pathogens*, 481–511.

Peraman, R., Sure, S. K., Dusthackeer, V. N. A., Chilamakuru, N. B., Yiragamreddy, P. R., Pokuri, C., Kutagulla, V. K., & Chinni, S. (2021). Insights on recent approaches in drug discovery strategies and untapped drug targets against drug resistance. *Future Journal of Pharmaceutical Sciences*, *7*(1), 56.

Ponte-Sucre, A., Gamarro, F., Dujardin, J.-C., Barrett, M. P., López-Vélez, R., García-Hernández, R., Pountain, A. W., Mwenechanya, R., & Papadopoulou, B. (2017). Drug resistance and treatment failure in leishmaniasis: A 21st century challenge. *PLoS Neglected Tropical Diseases*, *11*(12), e0006052.

Schiliro, C., & Firestein, B. L. (2021). Mechanisms of metabolic reprogramming in cancer cells supporting enhanced growth and proliferation. *Cells*, *10*(5), 1056.

Sharma, A., Gupta, V. K., & Pathania, R. (2019). Efflux pump inhibitors for bacterial pathogens: From bench to bedside. *Indian Journal of Medical Research*, *149*(2), 129–145.

Tang, K. W. K., Millar, B. C., & Moore, J. E. (2023). Antimicrobial resistance (AMR). *British Journal of Biomedical Science*, *80*, 11387.

Tarannum, A., Rodríguez-Almonacid, C. C., Salazar-Bravo, J., & Karamysheva, Z. N. (2023). Molecular mechanisms of persistence in protozoan parasites. *Microorganisms*, *11*(9), 2248.

Vasan, N., Baselga, J., & Hyman, D. M. (2019). A view on drug resistance in cancer. *Nature*, *575*(7782), 299–309.

Vitiello, A., Ferrara, F., Boccellino, M., Ponzo, A., Cimmino, C., Comberiati, E., Zovi, A., Clemente, S., & Sabbatucci, M. (2023). Antifungal drug resistance: an emergent health threat. *Biomedicines*, *11*(4), 1063.